A Study of the Recombination of IO with NO_2 and the Stability of INO_3: Implications for the Atmospheric Chemistry of Iodine

B. J. Allan and J. M. C. Plane*

School of Environmental Sciences, University of East Anglia, Norwich, NR4 7TJ, United Kingdom

Received: January 14, 2002; In Final Form: June 17, 2002

The recombination reaction between IO and NO_2 was studied over a large range of temperature (216−474 K) and pressure (20−760 Torr). IO, produced by the pulsed photolysis at 193 nm of NO_2 to yield O in the presence of CF_3I, was probed at 445.0 nm [IO($A^2\Pi_{3/2} - X^2\Pi_{3/2}$), (2,0)] and monitored by nonresonant LIF at 458.6 nm [IO($A^2\Pi_{3/2} - X^2\Pi_{3/2}$), (2,1)]. The resulting rate coefficients were then fitted by RRKM theory, using molecular parameters and a heat of formation for INO_3 ($\Delta H^\circ_{f,0} = 70 \pm 16$ kJ mol^{-1}, best fit value 80 kJ mol^{-1}) derived from quantum calculations at the B3LYP/6-311+g(2d,p) level. This yielded $k_{rec,0} = (1.3 \pm 0.2) \times 10^{-30}$ $(T/300\ K)^{-(4.5\pm0.6)}$ cm^6 molecule^{-2} s^{-1}, $k_{rec,\infty} = (6.5 \pm 1.0) \times 10^{-12}$ $(T/300\ K)^{-(1.3\pm0.8)}$ cm^3 molecule^{-1} s^{-1}, and $F_c = 0.57$, over the experimental range of temperature and pressure. The RRKM calculations, in conjunction with measurements made at 474 K, were used to determine the rate of thermal dissociation of INO_3 for the conditions of the lower atmosphere: $k_{diss}(240-305\ K, 760\ Torr) = 1.1 \times 10^{15} \exp(-12060/T)$ s^{-1}, with an upper limit about a factor of 2 higher. The atmospheric significance of these results is discussed briefly.

Introduction

Recent observations of the iodine monoxide (IO) and dioxide (OIO) radicals in the marine boundary layer provide direct evidence for the participation of gaseous inorganic iodine in tropospheric photochemistry.[1−3] The major source of atmospheric iodine appears to be biogenic iodocarbons, such as CH_2I_2 and CH_3I, which evade from the open ocean and coastal waters.[4] These photolyze to yield I atoms, which then react with O_3 to form IO. Of particular interest is the potential role of iodine in the destruction of tropospheric ozone via three catalytic cycles initiated by the reactions of IO with HO_2, NO_2, and itself.[5−8]

In this paper we will focus on ozone depletion by the cycle involving iodine nitrate (INO_3):

$$IO + NO_2 (+M) \rightarrow INO_3 \quad (1)$$

$$INO_3 + h\nu \rightarrow I + NO_3 \quad (2a)$$

$$\rightarrow IO + NO_2 \quad (2b)$$

$$INO_3 (+M) \rightarrow IO + NO_2 \quad (-1)$$

$$\rightarrow I + NO_3 \quad (3)$$

$$I + O_3 \rightarrow IO + O_2 \quad (4)$$

O_3 depletion will be significant only if I is the dominant photolysis product of INO_3 (reaction 2a rather than 2b), because I will go on to react with O_3 to reform IO through reaction 4. In fact, there appears to be only one preliminary report of the absorption cross-section of INO_3 in the UV/near visible [D. Rowley, U. College London, personal communication], and the branching ratio between channels 2a and 2b remains to be studied. Note that even if channel 2a dominates, the NO_3 fragment formed will photolyze to $NO_2 + O$ with a branching ratio of 0.8,[9] which will largely cancel the ozone-depleting effect. Furthermore, INO_3 may thermally decompose (reactions −1 and 3) rapidly enough to compete with photolysis. However, as we have discussed recently,[8] this is difficult to evaluate because the two estimates[6,10,11] of k_{-1} differ by nearly an order of magnitude.

In this paper we will report an experimental study of reaction 1 using a pulsed photolysis/laser induced fluorescence technique. This reaction has been studied previously by five different groups,[12−16] with some significant discrepancies that will be described below. We will report kinetic data over a wider range of pressure and temperature than in the earlier work, including measurements at elevated temperatures in order to investigate the thermal decomposition of INO_3. The experimental results will then be modeled using RRKM theory combined with quantum calculations on INO_3.

Experimental Section

Figure 1 is a schematic diagram of the pulsed laser photolysis/laser induced fluorescence (PLP/LIF) apparatus used to study these reactions. IO radicals were produced in the stainless steel reactor by the pulsed photolysis of a mixture of NO_2 and CF_3I in N_2 bath gas:

$$NO_2 + h\nu \rightarrow NO + O(^3P) \quad (5)$$

$$O + CF_3I \rightarrow IO + CF_3 \quad (6)$$

The photolysis of NO_2 was performed using an ArF excimer laser at 193 nm (Lambda Physik Compex 201, repetition rate = 5 Hz, fluence = $(0.1-2.6) \times 10^{16}$ cm^{-2}), since neither NO_2 nor CF_3I have particularly large cross-sections at this wavelength.[9,17] An excess of NO_2 was used allowing the IO formed to react primarily with the remaining NO_2 in the reactor. The laser fluence was limited so that less than 0.6% of the NO_2

* Corresponding author. E-mail: j.plane@uea.ac.uk. Fax: (44) 1603 507719.

10.1021/jp020089q CCC: $22.00 © 2002 American Chemical Society
Published on Web 08/16/2002

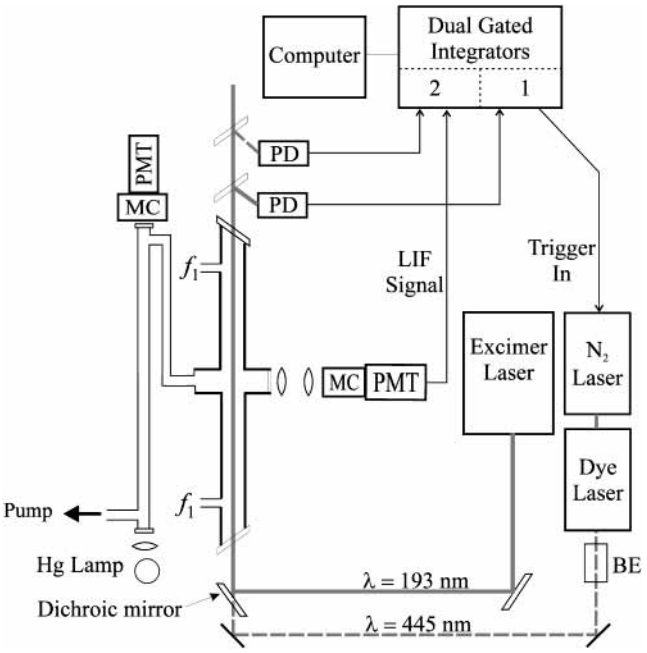

Figure 1. Schematic diagram of the pulsed laser photolysis/laser induced fluorescence apparatus: **BE**, beam expander; f_1, flow of reagent/bath gas mixture (≈ 250 sccm); **MC**, monochromator; **PMT**, photomultiplier tubes; **PD**, fast photodiode.

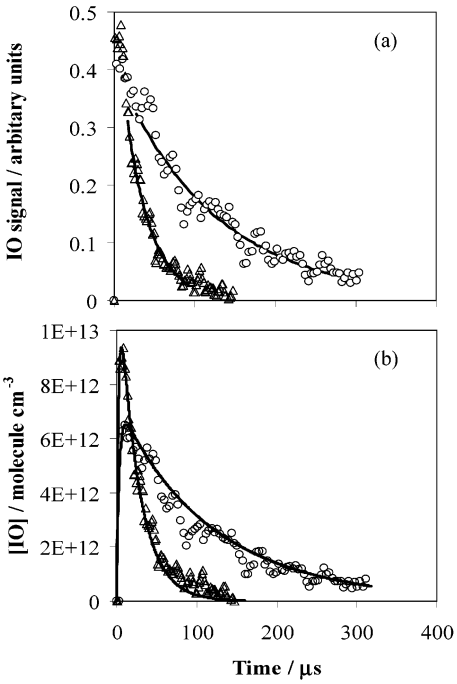

Figure 2. Time-resolved decays of the LIF signal from IO probed at 445.0 nm [IO($A^2\Pi_{3/2}-X^2\Pi_{3/2}$), (2,0)] and detected by the nonresonant LIF signal at 458.6 nm [IO($A^2\Pi_{3/2}-X^2\Pi_{3/2}$), (2,1)]. (a) LIF decays at 300 K and 760 Torr for $[NO_2] = 4.5 \times 10^{15}$ (circles) and 10.9×10^{15} (triangles) molecules cm^{-3}. The solid curves are fits of the form $A \exp(-k't)$ to the data points, yielding $k' = 11840$ and 37400 s^{-1}, respectively. (b) LIF decays as in (a) plotted with, and scaled to, the modeled output of IO (solid lines).

was photolyzed. This was necessary to limit the concentration of NO produced in reaction 5, since IO reacts relatively rapidly with IO.[9] The concentrations of CF_3I and NO_2 used in these experiments ranged from $(7.2-65) \times 10^{15}$ and $(0.3-45) \times 10^{15}$ molecule cm^{-3}, respectively, and $[CF_3I]$ was less than 1% of $[N_2]$ (except for two low-pressure experiments where it was less than 3%).

IO was probed at 445 nm, the band head of the (2,0) band in the IO($A^2\Pi_{3/2}-X^2\Pi_{3/2}$) system, using a nitrogen-pumped dye laser (laser dye Coumarin 450, pulse energy 20 μJ; bandwidth = 0.04 nm). The nonresonant LIF signal at $\lambda = 458.6$ nm [IO($A^2\Pi_{3/2} - X^2\Pi_{3/2}$, (2,1)] was detected by a fast photomultiplier tube (PMT) after being collected by a pair of lenses and focused through a 0.9 nm resolution monochromator (Optometrics Corp., Model MC1-02). The LIF signal was collected by a gated integrator with a 20 ns wide gate. Note that IO($A^2\Pi_{3/2}$) is largely predissociative, and its lifetime is only 9 ns.[18] Thus quenching by the bath gas was found to be negligible up to 1 atm of N_2. As shown in Figure 1, a second gated integrator, triggered by the excimer laser pulse, was used to trigger the probe laser after a scanned time delay controlled by a microcomputer. The excimer laser and dye laser beams were aligned to be collinear along the cylindrical axis of the reaction chamber. The chamber was cooled from room temperature down to 216 K by circulating chilled methanol through copper tubing wound around the outside of the chamber, or else heated to 474 K with electrical heating tape. The temperature of the gas inside the chamber, at the point from which the LIF was observed, was measured with a retractable thermocouple.

The concentration of NO_2 was monitored downstream of the reactor by optical absorption of the 435.833 nm line from a low-pressure mercury lamp (Figure 1). This was measured in a 1 m path length absorption cell with a second 0.9 nm resolution monochromator and PMT. The absorption cross section of NO_2 was taken to be 6.42×10^{-19} cm^2 at 435.8 nm and 298 K.[9] The dimerization of NO_2 to N_2O_4 at low temperatures was corrected for using the equilibrium constant from ref 9: at the lowest temperature of 216 K, the NO_2 concentration in the reactor was reduced by 25−33%.

Materials. CF_3I (99% pure, Aldrich), and N_2 (99.9999%, pure Air products) were used without further purification. NO_2 (99.5% pure, Air Products) was purified to remove NO using an ethanol/liquid N_2 slush bath.

Results

In the case of reaction 1, where the reagent NO_2 was in a large excess over IO, the removal of IO should be described approximately by the pseudo first-order decay coefficient,

$$k' \approx k_{\text{diff,IO}} + k_1[NO_2] + 2k_{\text{IO+IO}}[IO] + k_{\text{IO+NO}}[NO] \quad \text{(I)}$$

where the term $k_{\text{diff,IO}}$ describes the diffusion of IO out of the volume defined by the dye laser beam and within the field of view of the PMT; k_1 is the second-order rate coefficient for the recombination reaction 1 at a particular pressure; $k_{\text{IO+IO}}$ is the rate coefficient for the self-reaction of IO; and $k_{\text{IO+NO}}$ is the rate coefficient for the reaction between IO and NO. The experimental conditions were set to minimize the losses of IO from the self-reaction and the reaction with NO. To keep the last term in equation I approximately constant during an experimental run as $[NO_2]$ was varied, the excimer laser fluence was also varied in an opposite sense so that a roughly constant amount of NO was produced from the photolysis of NO_2.

Figure 2a illustrates two time-resolved decays of the LIF signal from IO in the presence of the lowest and highest concentrations of NO_2 used when studying reaction 1 at 760 Torr and 300K (see Table 1). The LIF decays are well fitted by a single exponential form after an appropriate time delay, as shown by the solid lines in Figure 2a. As described below, the resulting k' were then corrected using a kinetic model for the

TABLE 1: Experimental Determination of k_1 as a Function of Temperature and Pressure (quoted uncertainty is 1σ)

T/K	*P*/Torr	k_1 (corrected) /10^{-12} cm^3 molecule^{-1} s^{-1}	*T*/K	*P*/Torr	k_1 (corrected) /10^{-12} cm^3 molecule^{-1} s^{-1}
216	40	3.14 ± 0.23	278	552	3.89 ± 0.17
218	80	4.18 ± 0.40	278	650	4.04 ± 0.16
216	120	5.01 ± 0.22	278	762	4.30 ± 0.41
218	200	5.64 ± 0.45	300	32	0.66 ± 0.04
221	300	6.23 ± 0.18	300	40	0.80 ± 0.06
232	20	1.56 ± 0.15	300	84	1.37 ± 0.07
232	40	2.28 ± 0.23	301	120	1.61 ± 0.05
232	70	3.11 ± 0.07	301	200	1.89 ± 0.11
232	120	3.99 ± 0.59	302	400	2.96 ± 0.27
232	200	4.69 ± 0.69	302	550	3.37 ± 0.26
252	40	1.38 ± 0.04	301	650	3.63 ± 0.20
253	80	2.38 ± 0.07	301	760	3.71 ± 0.43
254	120	2.83 ± 0.18	342	40	0.51 ± 0.04
253	200	3.34 ± 0.78	336	120	1.11 ± 0.09
253	300	4.50 ± 0.34	375	40	0.34 ± 0.02
250	400	5.13 ± 0.48	376	120	0.75 ± 0.06
279	30	1.08 ± 0.15	372	300	1.29 ± 0.11
278	40	1.30 ± 0.07	429	40	0.22 ± 0.05
278	80	1.49 ± 0.10	430	120	0.34 ± 0.04
279	120	2.17 ± 0.13	422	300	0.74 ± 0.06
279	200	2.59 ± 0.12	473	40	0.13 ± 0.02
279	300	3.02 ± 0.30	476	110	0.28 ± 0.01
279	400	3.36 ± 0.18	473	300	0.55 ± 0.06

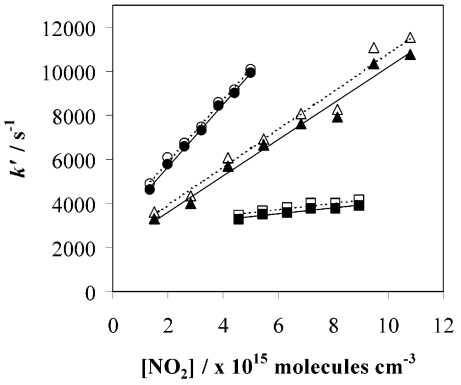

Figure 3. k' versus $[NO_2]$ for data obtained at 40 Torr and temperatures of 252 K (circles), 300 K (triangles), and 473 K (squares). Open symbols represent data not corrected for the self-reaction of IO and the reaction of IO with NO produced from the photolysis of NO_2. Filled symbols show the data corrected using a full kinetic model. The solid and dotted lines are linear regression fits through each set of data; the slopes of the solid lines give the corrected rate coefficients listed in Table 1.

contribution from the reactions of IO with itself and NO. The examples in Figure 2a correspond to k' values of 11840 s^{-1} (low NO_2) and 37400 s^{-1} (high NO_2), with contributions from IO and NO estimated to be 153 and 364 s^{-1} (low NO_2), and 333 and 606 s^{-1} (high NO_2), respectively. Therefore, the increase in k' illustrated in Figure 2a is indeed dominated by reaction 1.

Data sets were obtained by measuring k' as a function of $[NO_2]$ at constant pressure and temperature in the central chamber. Thus, $k_{diff,IO}$ appeared as the intercept in a plot of k' vs $[NO_2]$. Figure 3 shows examples of plots of k' versus $[NO_2]$, whose slopes provide initial estimates of k_1. The kinetic model used to refine these estimates employed a variable stepsize fourth-order Runge−Kutta integrator,[19] and included 26 reactions describing the chemistry taking place in the reactor (Table 2). The required model input for a particular experiment was the temperature, total pressure, $[CF_3I]$, $[NO_2]$, excimer laser fluence, and the initial estimate of k_1. From these data the temporal profile of IO was calculated. Figure 2b shows the modeled IO profiles for the two experiments in Figure 2a. There is very satisfactory agreement with the LIF profiles, which have been scaled to the model predictions.

The IO concentration obtained from the model, combined with k_{IO+IO}, was then used to calculate the contribution of the IO self-reaction to the total loss of IO during an experiment. For example, the modeled [IO] was in the range of (0.1−11.1) × 10^{12} molecules cm^{-3} over the time interval in which the decays were analyzed (the peak [IO] ranged from 7 × 10^{11} to 3.3 × 10^{13} molecules cm^{-3}, with the majority of IO concentrations not exceeding 1 × 10^{13} molecules cm^{-3}). Thus, the mean percentage contribution of the IO self-reaction to the total loss of IO was about 3%. The [NO] produced by the laser photolysis of NO_2 ranged from 1.5 × 10^{12} to 1.1 × 10^{14} molecules cm^{-3}, although the concentration was mostly kept below 1 × 10^{13} molecules cm^{-3}. The reaction of IO with NO contributed about 4% toward the total loss of IO.

The values of k' determined from the initial exponential fit to each of the decays in a particular experiment were then corrected for the losses due to the reactions of IO with itself and NO, producing corrected regression plots. Examples of these are also shown in Figure 3. The slopes of these plots yield k_1 as a function of temperature and pressure, as listed in Table 1. Figure 4 illustrates the pressure dependence of k_1 over a wide temperature range. The lower temperature limit of 216 K was constrained by cooling the reactor with chilled methanol. The upper limit of 474 K was determined by the decomposition of NO_2 on the hot reactor walls, which became too rapid above 500 K compared to the gas residence time.[33]

The 1σ uncertainties in k_1, obtained from the standard errors to the slopes of kinetic plots exemplified in Figure 3, are listed in Table 1 and plotted in Figure 4. The reproducibility of these second-order rate coefficients is estimated to be ±20%. This is based on the scatter of the experimental data points about the RRKM fits (see below), which are shown as solid lines in Figure 4, and corresponds roughly to the largest 2σ uncertainties in the experimental data points. The absolute uncertainties are estimated to be ±22%, which combines in quadrature the 20% statistical error with a 10% systematic error, comprising the sum of the uncertainties in the flow controllers (5%), the reactor pressure (4%), and the temperature (1%).

TABLE 2: Iodine Reaction Scheme Used in the Kinetic Model[a]

	reaction	rate coefficent	ref
(R1)	$IO + NO_2 + M \rightarrow INO_3 + M$	see text	this work
(R-1)	$INO_3 \rightarrow IO + NO_2$	see text	this work
(J5)	$NO_2 + h\nu$ (193 nm) $\rightarrow NO + O$	cross-section $= 2.5 \times 10^{-19}$ cm^{-2} (quantum yield assumed to be 1)	20
(R6)	$O + CF_3I \rightarrow IO + CF_3$	$1.3 \times 10^{-11}\, e^{(-266/T)}$	21
(J7)	$CF_3I + h\nu$ (193 nm) $\rightarrow CF_3 + I$	cross-section $= 2 \times 10^{-21}$ cm^{-2} (quantum yield assumed to be 1)	17
(R8)	$IO + IO \rightarrow OIO + I/I_2O_2$	$1.5 \times 10^{-11}\, e^{(500/T)}$	9
(R9)	$IO + NO \rightarrow I + NO_2$	$9.1 \times 10^{-12}\, e^{(240/T)}$	9
(R10)	$I + NO_2 + M \rightarrow INO_2 + M$	$k_0 = 3 \times 10^{-31} \times (T/300)^{-1}$ $k_\infty = 6.6 \times 10^{-11}$ $F_c = e^{(-T/650)} + e^{(-2600/T)}$	22
(R11)	$I + NO + M \rightarrow INO + M$	$k_0 = 1.8 \times 10^{-32} \times (T/300)^{-1}$ $k_\infty = 1.7 \times 10^{-11}$ $F_c = 0.6$	9
(R12)	$INO + INO \rightarrow I_2 + 2NO$	$8.4 \times 10^{-11}\, e^{(-2620/T)}$	9
(R13)	$INO_2 + INO_2 \rightarrow I_2 + 2NO_2$	$2.9 \times 10^{-11}\, e^{(-2600/T)}$	9
(R14)	$O + IO \rightarrow O_2 + I$	1.35×10^{-10} (at 296 K)	23
(R15)	$O + NO_2 \rightarrow NO + O_2$	$6.5 \times 10^{-12}\, e^{(120/T)}$	9
(R16)	$O + NO_2 + M \rightarrow NO_3 + M$	$k_0 = 9 \times 10^{-32} \times (T/300)^{-2}$ $k_\infty = 2.2 \times 10^{-11}$ $F_c = 0.6$	9
(R17)	$O + I_2 \rightarrow IO + I$	1.4×10^{-10}	9
(R18)	$O + NO + M \rightarrow NO_2 + M$	$k_0 = 9 \times 10^{-32} \times (T/298)^{-1.5}$ $k_\infty = 3 \times 10^{-11}$ $F_c = 0.6$	9
(R19)	$I + I + M \rightarrow I_2 + M$	$6.14 \times 10^{-34} \times (T/298)^{0.073} \times e^{(7430/8.314T)}$	24
(R20)	$CF_3 + NO_2 \rightarrow CF_2O + FNO$ $\rightarrow CF_2O + F + NO$	1.75×10^{-11} (at 298 K)	25
(R21)	$CF_3 + NO + M \rightarrow CF_3NO + M$	$k_0 = 3.2 \times 10^{-29} \times (T/298)^{-3.4}$ $k_\infty = 2 \times 10^{-11}$ $F_c = 0.6$	26
(R22)	$CF_3 + CF_3 + M \rightarrow C_2F_6 + M$	3.9×10^{-12} (at 296 K)	27
(R23)	$CF_3NO + O \rightarrow$ products	$4.54 \times 10^{-12} e^{(-560/T)}$	28
(R24)	$CF_3 + O \rightarrow CF_2O + F$	3.32×10^{-11}	29
(R25)	$CF_3 + O_2 + M \rightarrow CF_3O_2 + M$	$k_0 = 3 \times 10^{-29} \times (T/298)^{-4}$ $k_\infty = 4 \times 10^{-12} \times (T/300)^{-1}$ $F_c = 0.6$	9
(R26)	$CF_3 + I \rightarrow CF_3I$	$3 \times 10^{-11}\, e^{(-200/T)}$ (in Argon)	30
(R27)	$CF_3 + CF_3\, I \rightarrow C_2F_6 + I$	3×10^{-16} (upper limit at 298 K)	31
(R28)	$CF_3O_2 + NO_2 + M \rightarrow CF_3O_2NO_2 + M$	$k_0 = 3 \times 10^{-29} \times (T/298)^{-4}$ $k_\infty = 4 \times 10^{-12} \times (T/300)^{-1}$ $F_c = 0.6$	9
(R29)	$CF_3O + NO \rightarrow CF_2O + FNO$	$3.7 \times 10^{-11}\, e^{(110/T)}$	9
(R30)	$CF_3O_2 + NO \rightarrow CF_3O + NO_2$	$5.4 \times 10^{-12}\, e^{(320/T)}$	9
(R31)	$F + CF_3I \rightarrow CF_3 + IF$	1.2×10^{-10}	32

[a] Units: bimolecular reactions, cm^3 molecule^{-1} s^{-1}; termolecular reactions, cm^6 molecule^{-2} s^{-1}, calculated using the formalism in ref 9, where $k = ((k_0\,[M]/(1 + k_0[M]/k_\infty)) \times F_c^n)$, $F_c = 0.6$ and $n = \{1 + (\log (k_0\,[M]/k_\infty))^2\}^{-1}$.

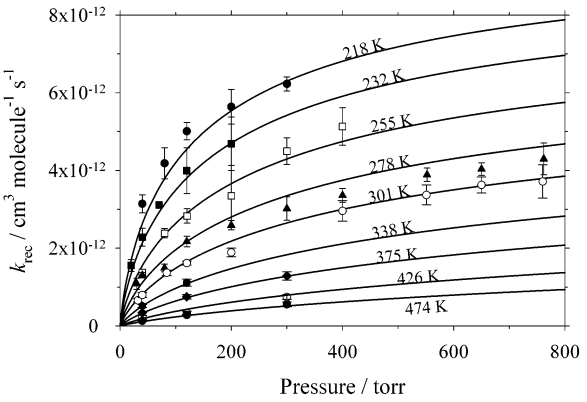

Figure 4. k_{rec} vs [M] at nine temperatures between 218 and 474 K, demonstrating that reaction 1 is in the falloff region. The individual rate coefficients are plotted with the 1σ standard errors from linear regression fits to kinetic plots of the type illustrated in Figure 3. The solid curves are fits of RRKM theory to the data at each temperature.

Ab Initio Quantum Calculations

To interpret these experimental results, a set of quantum calculations was carried out on IO, NO_2, and INO_3. The hybrid density functional/Hartree−Fock B3LYP method was employed from within the Gaussian 98 suite of programs.[34] For iodine, we used a 6-311G basis set, supplemented with d, f, and diffuse s and p functions, that has been developed recently and tested extensively by comparing the calculated properties of a variety of small iodine-containing molecules against experimental data.[35] For nitrogen and oxygen, the standard 6-311+g(2d,p) triple-ζ basis set was used. At this level of theory, the expected uncertainty in the calculated reaction enthalpy should be ±16 kJ mol^{-1}.[36]

The molecular geometries of IO, NO_2, and INO_3 were first optimized and checked for wave function stability. Their calculated dipole moments, rotational constants, vibrational frequencies, and heats of formation are listed in Table 3 and compared with experiment where possible. For I($^2P_{3/2}$) and IO($^2\Pi_{3/2}$), an empirical spin−orbit splitting correction was made, as described in the footnotes to Table 3. Figure 5 illustrates the geometry of INO_3, which was found to be a planar molecule. The ab initio vibrational frequencies of INO_3 are in good accord with those reported by Barnes et al.[11] (Table 3). In the case of IO and NO_2, the theoretical bond lengths, dipole moments, vibrational frequencies, and heats of formation are in generally

TABLE 3: Calculated Molecular Parameters and Heats of Formation for IO, NO_2, and INO_3 Using B3LYP Hybrid Density Functional Hartree−Fock Theory (experimental values where available shown in brackets for comparison)

species	geometry[a]	dipole moment[b]	rotational constants[c]	vibrational frequencies[d]	$\Delta H°_{f,0}$ [e]
$IO(X^2\Pi_{3/2})$	r(I−O) = 1.9011 [1.8677[f]]	2.52 [2.45[g]]	9.84 [10.2[f]]	649 [682[f]]	132 ± 16[h] [118 ± 5[i]]
$NO_2(^2A_1)$	r(N−O) = 1.194 [1.197[j]] ∠(O−N−O) = 134.37° [134.25°[j]]	0.347 [0.316[g]]	242.1 [239.0[j]] 13.04 [12.95[j]] 12.38 [12.26[j]]	761 [757[j]] 1381 [1358[j]] 1672 [1666[j]]	33.2 ± 8[k] [35.9[j]]
$INO_3(^1A')$	see figure 5	2.57	12.4, 1.30, 1.18	114, 177, 366, 588 [580[l]], 728, 752, 826 [815[l]] 1310 [1276[l]] 1703 [1673[l]]	70.3 ± 16[m] 70.5± 16[n]

[a] Bond distances in Å. [b] In Debye (= 3.336 × 10^{-30} Cm). [c] In GHz (1 GHz = 0.033 cm^{-1}). [d] In cm^{-1}. [e] In kJ mol^{-1}. [f] Ref 37. [g] Ref 38. [h] Using ab initio D_0(I−O) = 222 kJ mol^{-1} at the B3LYP/6-311+G(2d,p) level, including spin−orbit corrections of −30.3 kJ mol^{-1} for $I(^2P_{3/2})$ [ref 37] and −8.4 kJ mol^{-1} for $IO(^2\Pi_{3/2})$ [ref 39], and experimental $\Delta H°_{f,0}$(I) = 107.2 and $\Delta H°_{f,0}$(O)= 246.8 kJ mol^{-1} [ref 40]. [i] Experimental result from ref 41. [j] Ref 40. [k] Ab initio calculation at the B3LYP/6-311+G(2d,p) level. [l] Ref 11. [m] Using ab initio $D_0(IO-NO_2)$ = 94.9 kJ mol^{-1} calculated at the B3LYP/6-311+G(2d,p) level, with the ab initio $\Delta H°_{f,0}$ for IO and NO_2 above. [n] Using ab initio $D_0(I-NO_3)$ = 102.8 kJ mol^{-1} and $\Delta H°_{f,0}(NO_3)$ = 68.8 kJ mol^{-1} calculated at the B3LYP/6-311+G(2d,p) level, with experimental $\Delta H°_{f,0}$(I).

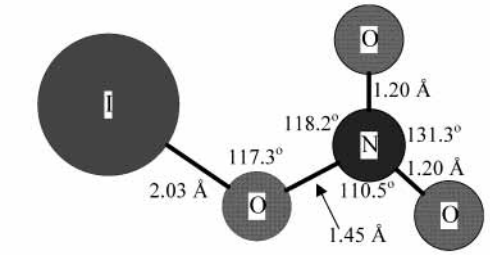

Figure 5. Geometry of INO_3 determined at the B3LYP/6-311+G(2d,p) level of theory. Note that the molecule is planar.

excellent agreement with experiment (Table 3). The enthalpy change at 0 K for the recombination of IO with NO_2 is −95 ± 16 kJ mol^{-1}, calculated from the data in Table 3. A survey of the potential energy surface showed that there is no barrier to recombination. This is to be expected since both reactants are radicals and, as Figure 5 shows, no bond rearrangements are needed to form INO_3 from IO and NO_2.

Discussion

Figure 3 shows that reaction 1 is well into the falloff region between 20 and 760 Torr. Therefore, to extrapolate k_1 outside the pressure and temperature regime that was accessible with the experimental technique used in this study, and to estimate k_{-1} for the thermal dissociation of INO_3, we have applied RRKM theory using the Master Equation (ME) formalism developed by De Avillez Pereira et al.[42] We have recently described the application of this formalism,[43] so only a brief description is given here. The reaction is assumed to proceed via the formation of an excited adduct (INO_3*), which can either dissociate or be stabilized by collision with the third body (N_2). The energy of the adduct was therefore divided into a contiguous set of grains (width 30 cm^{-1}), each containing a bundle of rovibrational states. Each grain was then assigned a set of microcanonical rate coefficients for dissociation, which were determined using inverse Laplace transformation[42] to link them directly to $k_{rec,\infty}$, the high-pressure limit recombination coefficient. In the present case, $k_{rec,\infty}$ was expressed in the form $A^\infty(T/300\ K)^n$.

The density of states of the adduct was calculated using a combination of the Beyer−Swinehart algorithm[44] for the vibrational modes (without making a correction for anharmonicity), and a classical densities of states treatment for the rotational modes. The molecular parameters listed in Table 3 were used. The ME describes the evolution with time of the grain populations of the adduct. The probability of collisional transfer between grains was estimated using the exponential down model,[44] where the average energy for downward transitions, $<\Delta E>_{down}$, was set to be 500 cm^{-1} for N_2 at 300 K. The probabilities for upward transitions were calculated by detailed balance. To use the ME to simulate irreversible stabilization of the adduct, an absorbing boundary was set 24 kJ mol^{-1} below the energy of the reactants, so that collisional energization from the boundary to the threshold was highly improbable.

The ME was expressed in matrix form[42] and then solved to yield $k_{1,calc}$, the recombination rate constant at a specified pressure and temperature. To fit $k_{1,calc}$ to the experimental data in Table 1, six adjustable parameters were allowed. These were E_0, the binding energy between IO and NO_2; the parameters A^∞ and n which define $k_{rec,\infty}$; α, which defines the T^α dependence of $<\Delta E>_{down}$; and σ and ϵ/k which describe the intermolecular potential between the adduct and N_2, used to calculate their collision frequency.[45] These parameters were varied in a simple grid search to minimize χ^2, defined as

$$\chi^2 = \sum_i^N \left(\frac{k^i_{1,meas} - k^i_{1,calc}}{\sigma_i} \right)^2 \qquad \text{(II)}$$

i.e., the sum over N (= 46) experimental points of the squared difference between the measured $k^i_{1,meas}$ (with statistical uncertainty σ_i in Table 1) and the modeled value $k^i_{1,calc}$.

The best fit values are: E_0 = 105 kJ mol^{-1}; $A^\infty = 6.46 \times 10^{-12}$ cm^3 $molecule^{-1}$ s^{-1}; $n = -1.32$; $\alpha = -1.15$; σ = 5.7 Å; and ϵ/k = 550 K. Note that E_0 is well within the expected uncertainty of the binding energy between IO and NO_2, calculated above. The satisfactory fit of RRKM theory to the experimental data for reaction 1 is illustrated in Figure 4 (note that the 1σ statistical uncertainties of $k_{1,meas}$ are plotted). The largest deviation between $k_{1,calc}$ and $k_{1,meas}$ is 21.7%, and the average deviation is 7.2%. Also, 87% of the $k_{1,calc}$ lie within the 2σ statistical uncertainties of $k_{1,meas}$, and all points lie within the absolute uncertainty (±22%).

To extrapolate k_1 over a large range of temperature (200−600 K) and pressure (0−1000 Torr), we have fitted the RRKM

TABLE 4: Low and High Pressure Limiting Rate Coefficients for the Reaction between IO and NO_2 in N_2

$k_{rec,0}$(300 K) /10^{-31} cm^6 molecule^{-2} s^{-1}	n[a]	$k_{rec,8}$(300 K) /10^{-11} cm^3 molecule^{-1} s^{-1}	m[b]	F_c	P/Torr	T/K	ref
4.3 ± 0.2[c]		1.6 ± 0.8			35−404	277−303	12
7.7 ± 1.9	−5.0	$1.6^{+1.6}_{-0.8}$	0	0.4	40−754	254−354	13
7.9 ± 2.2[d]					1.2−2.1	298	14
2.5 ± 0.1[e]	−2.6				1−6	290−350	15
13 ± 2	-4.4 ± 0.6	0.65 ± 0.1	-1.3 ± 0.8	0.57	20−760	216−474	this work

[a] $k_{rec,0}$ varies as $(T/300\ K)^n$. [b] $k_{rec,8}$ varies as $(T/300\ K)^m$. [c] Determined at 277 K only. [d] Determined at 298 K only. Helium used as the bath gas, relative efficiency of N_2/He taken as 2.2/1 [ref 14]. [e] O_2 used as the bath gas, relative efficiency of N_2/O_2 taken as 1/0.7 [ref 15].

results to the conventional Lindemann expression modified by a broadening factor F_c:[9]

$$k_1 = \frac{k_{rec,0}[M]}{1 + \frac{k_{rec,0}[M]}{k_{rec,\infty}}} F_c^{\,K} \qquad \text{(III)}$$

where

$$K = \frac{1}{\left\{1 + \left(\log_{10}\left(\frac{k_{rec,0}[M]}{k_{rec,\infty}}\right)\right)^2\right\}}$$

where the low-pressure limiting rate coefficient $k_{rec,0} = (1.3 \pm 0.2) \times 10^{-30}\ (T/300\ K)^{-(4.5\pm0.6)}$ cm^6 molecule^{-2} s^{-1}, $k_{rec,\infty} = (6.5 \pm 1.0) \times 10^{-12}\ (T/300\ K)^{-(1.3\pm0.8)}$ cm^3 molecule^{-1} s^{-1}, and $F_c = 0.57$.

Comparison with Previous Measurements of k_1. Table 4 compares the present results with four previous studies of reaction 1. In each case the range of experimental pressure and temperature is listed, along with estimates of $k_{rec,0}$ and $k_{rec,\infty}$ (where applicable). The earliest study was by Jenkin and Cox,[12] who measured k_1 using a photochemical modulation technique. Daykin and Wine[13] employed a laser flash photolysis/long-path absorption technique to study reaction 1 over a large range of pressure and temperature. Maguin et al.[14] studied the reaction in a low-pressure discharge-flow system at 298 K. In comparing with our work with N_2 as the third body, we have multiplied their values of $k_{rec,0}$ measured in He by 2.2, as recommended by those authors. Finally, Larin et al.[15] used a flow reactor with indirect detection of IO via reduction with NO to I, which was monitored by atomic resonance fluorescence.

Figure 6 compares the present results with these previous studies, as well as the preliminary results from a new study by Blitz et al.,[16] who employed a flash photolysis/laser induced fluorescence technique similar to that used here. Figure 6a is a comparison of results over a range of pressure, at temperatures close to 300 K. This shows that the present study is in very good agreement with the results of Daykin and Wine[13] and Blitz et al.[16] between 20 and 760 Torr, and our RRKM fit extrapolates to be in satisfactory agreement with the low-pressure measurements of Maguin et al.[14] In contrast, the studies of Jenkins and Cox[12] and Larin et al.,[15] while in accord with each other, are about a factor of 2 lower than the other measurements. The possible reasons for the discrepancy with the study of Jenkins and Cox[12] have been discussed previously,[13,14] and we note that Larin et al.[15] employed an indirect detection of IO (see above) which may have compromised the measurement of k_1.

Figure 6b compares the temperature dependence of k_1 at a pressure of 100 Torr N_2, a pressure used in three previous studies.[12,13,16] Since our measurements were made at pressures of 80 and 120 Torr, we have shown our RRKM fit at 100 Torr for comparison with the earlier work. Over the common temperature range of 254−354 K our result agrees well with that of Daykin and Wine,[13] being about 20% higher and with a very similar temperature dependence. There is also satisfactory agreement with the preliminary measurements of Blitz et al.[16] Once again, however, the result of Jenkin and Cox[12] is substantially smaller.

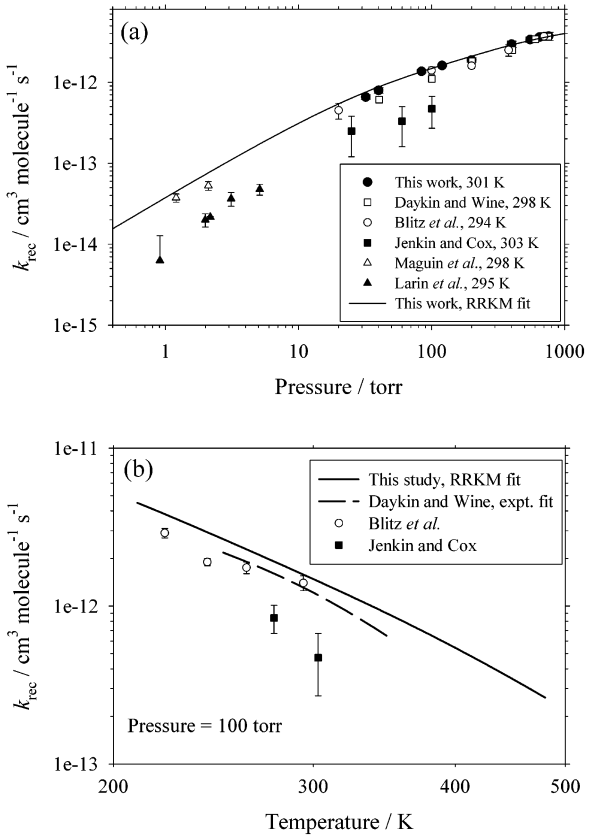

Figure 6. (a) Plot of k_{rec} vs [M] at 300 K, comparing the experimental data and RRKM fit from the present study with previous experimental work from Jenkin and Cox (ref 12), Daykin and Wine (ref 13), Maguin et al. (ref 14), Larin et al. (ref 15), and Blitz et al. (ref 16). (b) Plot of k_{rec} vs [T] at 100 Torr N_2, comparing the RRKM fit from the present study with previous experimental work.

Estimate of k_{-1} and Atmospheric Implications. To estimate k_{-1} for the thermal dissociation of INO_3 at atmospheric temperatures (<305 K), we now invert the RRKM fit to k_1. The effect of the uncertainty in seven parameters was considered: E_0, A^∞, n, $\langle\Delta E\rangle_{down}$, α, σ (the INO_3-N_2 collision cross-section), and $\nu_1(INO_3)$, the lowest vibrational frequency of INO_3. The individual uncertainty of each of these parameters was assigned to be that which caused χ^2 in equation II to double. A set of the seven parameters was then chosen by Monte Carlo sampling of each parameter, assuming a uniformly random distribution within each parameter's range of uncertainty. The value of $k_{1,calc}$ was then determined at three temperatures over the experimental pressure range. If $k_{1,calc}$ fell within $\pm 2\sigma$ of

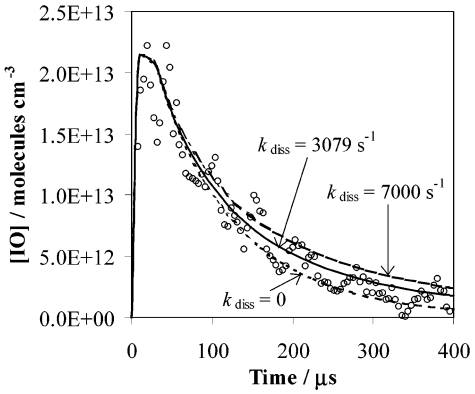

Figure 7. Temporal profile of LIF signal from IO observed during an experiment at 473 K and 300 Torr. The solid line indicates the modeled IO when k_{rec} and k_{diss} are set to the values derived from fitting the RRKM model to the complete data set on k_1. The dotted and dashed lines illustrate upper and lower limits to the model outputs obtained by setting k_{diss} for INO_3 to 0 and 7000 s^{-1} (see text for discussion).

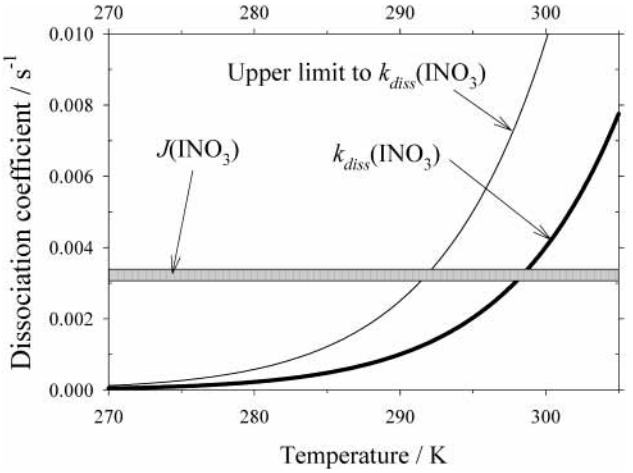

Figure 8. A comparison of the rates of removal of INO_3 from photolysis and thermal dissociation, as a function of temperature, for the conditions of the lower troposphere (pressure = 760 Torr).

$k_{1,meas}$ then this set of parameters was used to extrapolate $k_{1,calc}$ to a chosen temperature and pressure. This criterion allows for the fact that the fitted parameters are not all independent of each other. Using the values of E_0 and $\nu_1(INO_3)$ chosen by Monte Carlo sampling, $k_{-1,calc}$ was then determined by detailed balance with $k_{1,calc}$. The procedure was repeated until 200 successful Monte Carlo selections and extrapolations had been performed. The uncertainty in the extrapolated $k_{1,calc}$ and $k_{-1,calc}$ is then given by 2 standard deviations about the mean of the 200 estimates. This approach is a simplified (and less computer-intensive) variation of the Monte Carlo technique developed by Hessler.[46]

Applying this procedure indicates that the lower limit to E_0 is 102 kJ mol^{-1}, in accord with the ab initio estimate of $D_0(IO-NO_2) = 95 \pm 16$ kJ mol^{-1} (see above). For the highest temperature and pressure of the present study, $k_{-1,calc}$(473 K, 300 Torr) = 3079 s^{-1}. Figure 7 shows a satisfactory fit to the experimental LIF decay using with this value of $k_{-1,calc}$ in the kinetic model described earlier. Note that setting $k_{-1,calc}$ to zero produces a modeled decay that is too fast, showing that $k_{-1,calc}$ is starting to become significant at this temperature. Figure 7 also shows that when $k_{-1,calc}$ is increased to 7000 s^{-1}, then the decay becomes too slow. This corresponds to $D_0(IO-NO_2) >$ 101 kJ mol^{-1}, consistent with the Monte Carlo estimate above.

The Monte Carlo procedure yields a best estimate for the dissociation of INO_3 under atmospheric conditions of $k_{-1}(240-305$ K, 760 Torr) = $1.14 \times 10^{15} \exp(-12060/T)$ s^{-1}, with an upper limit of $1.50 \times 10^{15} \exp(-11890/T)$ s^{-1}. This is about a factor of 2 slower than the expression $2.07 \times 10^{15} \exp(-11859/T)$ s^{-1} that we used in our recent photochemical box model of atmospheric iodine,[8] where the preexponential factor was estimated by Jenkin et al.[6] and the temperature dependence by Chatfield and Crutzen.[10] The new expression for k_{-1} obtained here yields a value at 298 K of 3.0×10^{-3} s^{-1}, with an upper limit of 7.0×10^{-3} s^{-1}. This is about an order of magnitude lower than the rate of 3.2×10^{-2} s^{-1} reported by Barnes et al.,[11] who observed INO_3 by IR absorption spectroscopy and monitored its dark decay at 298 K. In fact, those authors made clear that the rapid decay of INO_3 they observed could have been due to other processes besides thermal dissociation, such as wall losses.

In the atmosphere, thermal dissociation of INO_3 will compete with photolysis (and possibly heterogeneous uptake).[8] The absorption cross-section of INO_3 has recently been measured in the near UV [D. Rowley, U. College London, personal communication]. Assuming that the structureless continuum corresponds to photolysis (reactions 2a and 2b), then a midday photolysis rate of $J(INO_3) = 3.2 \times 10^{-3}$ s^{-1} can be estimated.[8] Figure 8 illustrates the competition between photolysis and thermal dissociation, as a function of temperature. This shows that although these processes have comparable rates around 300 K, below 290 K photolysis should dominate and the iodine nitrate cycle can start to contribute to O_3 removal in the lower troposphere. Finally, it should be noted that although we have used N_2 as the third body in this study of reaction 1, for the purposes of atmospheric modeling it can be assumed[9] that the efficiency of O_2 is similar enough to N_2 for equation III to be applied to air.

Acknowledgment. This work was supported by the Natural Environment Research Council's program *Core Strategic Studies in Atmospheric Chemistry* (GST022718).

References and Notes

(1) Alicke, B.; Hebestreit, K.; Stutz, J.; Platt, U. *Nature* **1999**, *397*, 572.
(2) Allan, B. J.; McFiggans, G.; Plane, J. M. C.; Coe, H. *J. Geophys. Res.* **2000**, *105*, 14371.
(3) Allan, B. J.; McFiggans, G.; Plane, J. M. C. *Geophys. Res. Lett.* **2001**, *28*, 1945.
(4) Carpenter, L. J.; Sturges, W. T.; Penkett, S. A.; Liss, P. S.; Alicke, B.; Heibestreit, K.; Platt, U. *J. Geophys. Res.* **1999**, *104*, 1679.
(5) Chameides, W. L.; Davis, D. D. *J. Geophys. Res.* **1980**, *85*, 7383.
(6) Jenkin, M. E.; Cox, R. A.; Candeland, D. E. *J. Atmos. Chem.* **1985**, *2*, 359−375.
(7) Davis, D.; Crawford, J.; Liu, S.; McKeen, S.; Bandy, A.; Thornton, D.; Rowland, F. S.; Blake, D. *J. Geophys. Res.* **1996**, *101*, 2135.
(8) McFiggans, G.; Plane, J. M. C.; Allan, B. J.; Carpenter, L. J.; Coe, H.; O'Dowd C. *J. Geophys. Res.* **2000**, *105*, 14371.
(9) DeMore, W. B.; Sander, S. P.; Golden, D. M.; Hampson, R. F.; Kurylo, M. J.; Howard, C. J.; Ravishankara, A. R.; Kolb, C. E.; Molina, M. J. *Chemical Kinetics and Photochemical Data for Use in Stratospheric Modeling*: *Evaluation 12*, Jet Propulsion Laboratory, California, 1997.
(10) Chatfield, R. B.; Crutzen, P. J. *J. Geophys. Res.* **1990**, *95*, 22319.
(11) Barnes, I.; Becker, K. H.; Starcke, J. *J. Phys. Chem.* **1991**, *95*, 9736.
(12) Jenkin, M. E.; Cox, R. A. *J. Phys. Chem.* **1985**, *89*, 192.
(13) Daykin, E. P.; Wine, P. H. *J. Phys. Chem.* **1990**, *94*, 4528.
(14) Maguin, F.; Laverdet, G.; Le Bras, G.; Poulet, G. *J. Phys. Chem.* **1992**, *96*, 1775.
(15) Larin, I. K.; Nevozhai, D. V.; Spasskii, A. I.; Trofimova, E. M. *Kinet. Catal.* **1998**, *39*, 726.
(16) Blitz, M. A.; Dillon, T. J.; Heard, D. E.; Trought, I. D. *Proceedings of the16th International Symposium on Gas Kinetics*, Cambridge, U.K., 2000.
(17) Fahr, A.; Nayak, A. K.; Huie, R. E. *Chem. Phys.* **1995**, *199*, 275.
(18) Turnipseed, A. A.; Gilles, M. K.; Burkholder, J. B.; Ravishankara, A. R. *Chem. Phys. Lett.* **1995**, *242*, 427.

(19) Press, W. H.; Flannery, B. P.; Teukolsky, S. A.; Vetterling, W. T. *Numerical Recipes*: *The Art of Scientific Computing*; Cambridge University Press: New York, 1996.
(20) Bass, A. M.; Ledford, A. E., Jr.; Lauffer, A. H. *J. Res. NBS* **1976**, *80A*, 143.
(21) Hölscher, D.; Fockenberg, Chr.; Zellner, R. *Ber. Bunsen-Ges. Phys. Chem.* **1998**, *102*, 716.
(22) Atkinson, R.; Baulch, D. L.; Cox, R. A.; Hampson, R. F.; Kerr, J. A.; Troe, J. *J. Phys. Chem. Ref Data* **1992**, *21*, 1125.
(23) Canosa-Mas, C. E.; Flugge, M. L.; Shah, D.; Vipond, A.; Wayne, R. P. *J. Atmos. Chem.* **1999**, *34*, 153.
(24) Ip, J. K. K.; Burns, G. *J. Chem. Phys.* **1972**, *56*, 3155.
(25) Breheny, C.; Hancock, G.; Morrell, C. *Phys. Chem. Chem. Phys.* **2000**, *2*, 5105.
(26) Ley, L.; Masanet, J.; Caralp, F.; Lesclaux, R. *J. Phys. Chem.* **1995**, *99*, 1953.
(27) Vakhtin, A. B. *Int. J. Chem. Kinet.* **1996**, *28*, 443.
(28) Thorn, R. P.; Nicovich, J. M.; Cronkhite, J. M.; Wang, S.; Wine, P. H. *Int. J. Chem. Kinet.* **1995**, *27*, 369.
(29) Herron, J. T. *J. Phys. Chem. Ref. Data* **1988**, *17*, 967.
(30) Skorobogatov, G. A.; Slesar, O. N.; Torbin, N. D. *Vestn. Leningr. University Ser. 4*: *Fiz. Khim.* **1988**, *1*, 30.
(31) Andreeva, T. L.; Kuznetsova, S. V.; Maslov, A. I.; Sobel'man, I. I.; Sorokin, V. N. *High Energy Chem.* **1972**, *6*, 368.
(32) Bozzelli, J. W.; Kaufman, M. *J. Phys. Chem.* **1973**, *77*, 1748.
(33) Plane, J. M. C.; Rollason, R. J. *Phys. Chem. Chem. Phys.* **1999**, *1*, 1843.
(34) Frisch, M. J.; Trucks, G. W.; Schlegel, H. B.; Scuseria, G. E.; Robb, M. A.; Cheeseman, J. R.; Zakrzewski, V. G.; Montgomery, J. A., Jr.; Stratmann, R. E.; Burant, J. C.; Dapprich, S.; Millam, J. M.; Daniels, A. D.; Kudin, K. N.; Strain, M. C.; Farkas, O.; Tomasi, J.; Barone, V.; Cossi, M.; Cammi, R.; Mennucci, B.; Pomelli, C.; Adamo, C.; Clifford, S.; Ochterski, J.; Petersson, G. A.; Ayala, P. Y.; Cui, Q.; Morokuma, K.; Malick, D. K.; Rabuck, A. D.; Raghavachari, K.; Foresman, J. B.; Cioslowski, J.; Ortiz, J. V.; Baboul, A. G.; Stefanov, B. B.; Liu, G.; Liashenko, A.; Piskorz, P.; Komaromi, I.; Gomperts, R.; Martin, R. L.; Fox, D. J.; Keith, T.; Al-Laham, M. A.; Peng, C. Y.; Nanayakkara, A.; Gonzalez, C.; Challacombe, M.; Gill, P. M. W.; Johnson, B.; Chen, W.; Wong, M. W.; Andres, J. L.; Gonzalez, C.; Head-Gordon, M.; Replogle, E. S.; Pople, J. A. *Gaussian 98*, revision A.7; Gaussian, Inc.: Pittsburgh, PA, 1998.
(35) Glukhovtsev, M. N.; Pross, A.; McGrath, M. P. *J. Chem. Phys.* **1995**, *103*, 1878.
(36) Foresman, J. B.; Frisch, A. *Exploring chemistry with electronic structure methods*; Gaussian, Inc.: Pittsburgh, PA, 1996.
(37) Bekooy, J. P.; Meerts, W. L.; Dymanus, A. *J. Mol. Spectrosc.* **1983**, *102*, 320.
(38) *Handbook of Physics and Chemistry*, 78th ed.; Lide, D. R., Ed.; CRC Press: Boca Raton, 1997.
(39) Gilles, M. K.; Polak, M. L.; Lineberger, W. C. *J. Chem. Phys.* **1991**, *95*, 4723.
(40) Chase, M. W.; Davies, C. A.; Downey, J. R.; Frurip, D. J.; McDonald R. A.; Syverud, A. N.; *JANAF Thermochemical Tables*, 3rd ed., *J. Phys. Chem. Ref. Data* **1985**, *14*.
(41) Bedjanian, Y.; Le Bras, G.; Poulet, G. *J. Phys. Chem. A* **1997**, *101*, 4088.
(42) De Avillez Pereira, R.; Baulch, D. L.; Pilling, M. J.; Robertson, S. H.; Zeng, G. *J. Phys. Chem.* **1997**, *101*, 9681.
(43) Plane, J. M. C.; Rollason, R. J. *J. Phys. Chem. A* **2001**, *105*, 7047.
(44) Gilbert, R. G.; Smith, S. C. *Theory of Unimolecular and Recombination Reactions*; Blackwell: Oxford, 1990.
(45) Troe, J. *J. Chem. Phys.* **1977**, *66*, 4758.
(46) Hessler, J. P. *Int. J. Chem. Kinet.* **1997**, *29*, 803.